Enhancing propulsion performance of a flexible heaving foil through dynamically adjusting its flexibility

Chenglei Wang,[1] Feng Ren,[1] and Hui Tang[1, a)]

Research Center for Fluid-Structure Interactions, Department of Mechanical Engineering, The Hong Kong Polytechnic University, Kowloon, Hong Kong SAR, China

This study investigates how dynamically adjusting the bending stiffness of a heaving foil affects its propulsion performance in a flow of Reynolds number 200. The foil is forced to oscillate sinusoidally at the leading edge, and its bending stiffness is tuned in a square-wave manner. Such a fluid-structure interaction (FSI) problem is explored using an immersed boundary lattice Boltzmann method (IBLBM) based numerical framework. The results reveal that when the lower and upper bounds of the foil's time-dependent bending stiffness are moderate, the net thrust can be evidently enhanced compared to those in the corresponding constant-bending-stiffness cases, while the propulsion efficiency is not apparently ameliorated. The most significant enhancement is observed when the bending stiffness has lower and upper bounds of the same duration (i.e., a duty cycle of 1/2) and also it remains at the lower bound during stroke reversals (corresponding to an actuation phase angle of $\pi/2$). When the two bounds simultaneously increase or decrease, however, dynamically adjusting the bending stiffness fails to improve the net thrust. Through this study, competitions among various forces/moments, including the inertial force, tension force, bending moment and fluid loading, acting on the foil and their influences on the foil's dynamics are also unveiled.

a)h.tang@polyu.edu.hk

I. INTRODUCTION

Flapping motion is one of the most sophisticated thrust generation methods found in nature. Adopted by insects, birds and fishes, it is able to provide superior maneuverability and locomotor performance[1]. Due to the increasing interests in the micro air vehicles (MAVs), flapping motion has attracted more and more attentions recently. Thus far, numerous studies have been conducted to reveal the fundamental mechanisms of thrust generation of single/multiple foils undergoing flapping motion[2,3], or to investigate the influences of a series of key parameters, including the Strouhal number[4,5], reduced frequency[4,6], Reynolds number[7], aspect ratio[8], mass ratio[9,10] and complex motion[11,12] on flapping foil's aerodynamic/hydrodynamic performance. On these topics Shyy et al.[13,14] and Videler[15] have given comprehensive reviews.

As one of the most significant parameters, the flexibility affects the competitions among various forces/moments exerted on a flapping foil, thus influences the foil's dynamics and propulsion performance[9,12]. Hence, its effects have been extensively explored with different configurations[9,10,12,16,17]. For simplification, in most of the existing studies the foil's bending stiffness was assumed time-independent. This, nevertheless, is not always the case in nature, since the flexibility depends on the elastic properties of muscle tissue which can be modified with time. For instance, fishes can use their muscles to modulate their body stiffness in the course of cruising[18,19], and birds behave similarly when they steer the strength of their wing muscles during flight[20]. This difference indicates that the role played by the time-dependent bending stiffness in the propulsion performance of natural flyers and swimmers has rarely been explored and thus still remains unclear. To address this knowledge gap, this paper aims to investigate the effect of dynamically adjusting the bending stiffness on the propulsion performance of a foil heaving in a uniform flow. With the recent development of novel elastomer actuators[21,22], hopefully this study can provide some guidance on the design and operation of these actuators in the field of flapping-wing aerodynamics/hydrodynamics.

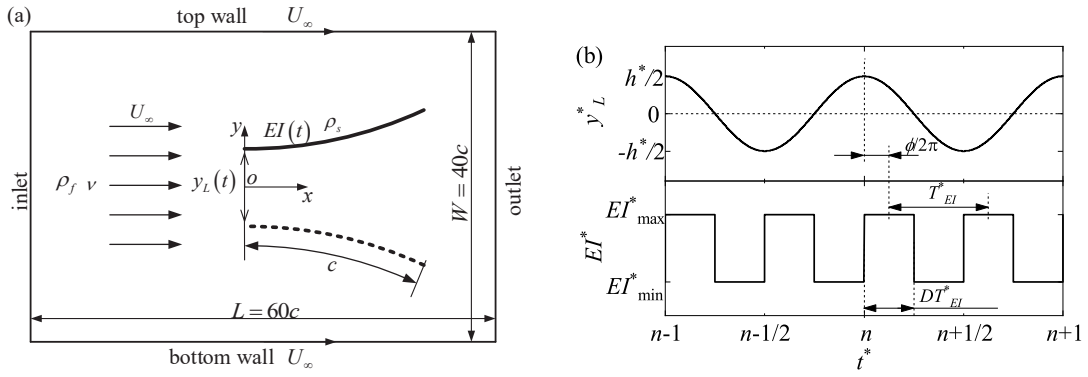

FIG. 1. Schematic of a flexible foil undergoing a pure heaving motion $y_L(t)$ prescribed by Equation 1, and the computational domain (not in scale) with implemented boundary conditions (a), and illustration for the definitions of the parameters of the time-dependent bending stiffness ($EI^*(t^*)$) (b).

II. PROBLEM DESCRIPTION AND METHODOLOGY

A. Problem description

In this study, a foil with chord length c, linear density ρ_s and time-dependent bending stiffness $EI(t)$ is immersed in a uniform flow of velocity U_∞, density ρ_f and kinematic viscosity ν, as shown in Figure 1(a). The foil undergoes a purely harmonic heaving motion which can be specified as

$$y_L(t) = \frac{h}{2}\cos(2\pi f t) \tag{1}$$

where y_L is the transverse displacement of the foil's leading edge, f the heaving frequency and h the heaving amplitude.

Assuming the foil as a clamped-free, inextensible elastic plate, its dynamics is governed by two nonlinear equations[23]

$$\rho_s \frac{\partial^2 \boldsymbol{X}}{\partial t^2} - \frac{\partial}{\partial s}\left(T_F \frac{\partial \boldsymbol{X}}{\partial s}\right) + \frac{\partial^2}{\partial s^2}\left(EI(t)\frac{\partial^2 \boldsymbol{X}}{\partial s^2}\right) = \boldsymbol{F}_f \tag{2}$$

$$\frac{\partial \boldsymbol{X}}{\partial s} \cdot \frac{\partial \boldsymbol{X}}{\partial s} = 1 \tag{3}$$

with boundary conditions

$$y(t,0) = y_L(t); \frac{\partial \boldsymbol{X}}{\partial s}(t,0) = (1,0) \qquad \text{imposed at the leading edge,}$$

and $$T_F(t,c) = 0; \frac{\partial^2 \boldsymbol{X}}{\partial s^2}(t,c) = \frac{\partial^3 \boldsymbol{X}}{\partial s^3}(t,c) = (0,0) \qquad \text{imposed at the trailing edge,}$$

where s is the Lagrangian coordinate along the foil, $\boldsymbol{X}$ the foil's position, T_F the tension force serving to satisfy the inextensible condition[23], and $\boldsymbol{F}_f$ the fluid loading acting on the foil.

The flow dynamics can be described by the incompressible Navier-Stokes equations

$$\frac{\partial \boldsymbol{v}}{\partial t} + \boldsymbol{v} \cdot \nabla \boldsymbol{v} = -\frac{1}{\rho_f} \nabla p + \nu \nabla^2 \boldsymbol{v} + \boldsymbol{f}_e \tag{4}$$

$$\nabla \cdot \boldsymbol{v} = 0 \tag{5}$$

where $\boldsymbol{v}$ is the flow velocity, p the pressure, ∇ the gradient operator, and $\boldsymbol{f}_e$ the external force per unit volume.

To parameterize this fluid-structure interaction (FSI) system, the freestream velocity (U_∞), chord length (c), fluid density (ρ_f) and heaving frequency (f) are chosen as repeating variables. Equations 1 to 5 can be non-dimensionalized as

$$y_L^*(t^*) = \frac{h^*}{2} \cos(2\pi t^*) \tag{6}$$

$$\frac{m^* k^2}{\pi^2} \frac{\partial^2 \boldsymbol{X}^*}{\partial t^{*2}} - \frac{\partial}{\partial s^*} \left(T_F^* \frac{\partial \boldsymbol{X}^*}{\partial s^*} \right) + \frac{\partial^2}{\partial s^{*2}} \left(EI^*(t^*) \frac{\partial^2 \boldsymbol{X}^*}{\partial s^{*2}} \right) = \boldsymbol{F}_f^* \tag{7}$$

$$\frac{\partial \boldsymbol{X}^*}{\partial s^*} \cdot \frac{\partial \boldsymbol{X}^*}{\partial s^*} = 1 \tag{8}$$

$$\frac{k}{\pi} \frac{\partial \boldsymbol{v}^*}{\partial t^*} + \boldsymbol{v}^* \cdot \nabla^* \boldsymbol{v}^* = -\nabla^* p^* + \frac{1}{\mathrm{Re}} \nabla^{*2} \boldsymbol{v}^* + \boldsymbol{f}_e^* \tag{9}$$

$$\nabla^* \cdot \boldsymbol{v}^* = 0 \tag{10}$$

For ease of reference, the definitions of all the dimensionless parameters in Equations 6 to 10 are elaborated in Table I.

Herein, the bending stiffness $EI^*(t^*)$ is assumed as a square wave function of time with a dimensionless period T_{EI}^*, a duty cycle D, a phase angle ϕ with respect to the foil's heaving motion, and lower and upper bounds EI_{min}^* and EI_{max}^*, as shown in Figure 1(b). By taking all these factors into account, it can be expressed as

$$EI^*(t^*) = \begin{cases} EI_{max}^* & \frac{\phi}{2\pi} + (i - \frac{D}{2}) T_{EI}^* \le t^* < \frac{\phi}{2\pi} + (i + \frac{D}{2}) T_{EI}^* \\ EI_{min}^* & \frac{\phi}{2\pi} + (i + \frac{D}{2}) T_{EI}^* \le t^* < \frac{\phi}{2\pi} + (i + 1 - \frac{D}{2}) T_{EI}^* \end{cases}, i = 0, 1, 2... \tag{11}$$

Note that when the duty cycle $D = 0$ or 1, the bending stiffness becomes time-independent, i.e., $EI^* \equiv EI_{min}^*$ or EI_{max}^*. More detailed definitions for all the above parameters are given in Table I.

TABLE I. Definitions and selected values of dimensionless parameters in this study.

Dimensionless parameter	Definition	Values
Duty cycle	$D = PW/T_{EI}$	0,1/8,1/4,**1/2**,3/4,7/8,1
Bending stiffness	$EI^* = EI/\rho_f U_\infty^2 c^3$	-
Maximum bending stiffness	$EI^*_{max} = EI_{max}/\rho_f U_\infty^2 c^3$	1,**3**,9
Minimum bending stiffness	$EI^*_{min} = EI_{max}/\rho_f U_\infty^2 c^3$	1/3,**1**,3
Heaving frequency	$f^* = f/f_N = (2\pi/k_1^2)\sqrt{m^* k^2/\pi^2 EI^*}$	-
External force per unit volume	$\boldsymbol{f}_e^* = \boldsymbol{f}_e c/U_\infty^2$	-
Fluid loading	$\boldsymbol{F}_f^* = \boldsymbol{F}_f/\rho_f U_\infty^2$	-
Heaving amplitude	$h^* = h/c = St\pi/k$	0.6
Reduced frequency	$k = \pi f_b c/U_\infty$	$\pi/2$
Mass ratio	$m^* = \rho_s/\rho_f c$	1
Pressure	$p^* = p/\rho_f U_\infty^2$	-
Reynolds number	$Re = U_\infty c/\nu$	200
Lagrangian coordinate	$s^* = s/c$	-
Strouhal number	$St = f_b h_b/U_\infty$	0.3
Time	$t^* = tf$	-
Variation period of EI^*	$T^*_{EI} = T_{EI} f$	1/2
Tension force	$T_F^* = T_F/\rho_f U_\infty^2 c$	-
Velocity	$\boldsymbol{v}^* = \boldsymbol{v}/U_\infty$	-
Foil's position	$\boldsymbol{X}^* = \boldsymbol{X}/c$	-
Leading-edge y-displacement	$y_L^* = y_L/c$	Prescribed by Equation 6
Phase angle	ϕ	0, $\pi/4$, $\boldsymbol{\pi/2}$, $3\pi/4$, π
Derivative operator	$\nabla^* = c\nabla$	-

[a] PW is the pulse width of the square waveform. Herein, it refers to a single duration when the bending stiffness remains larger.

[b] f_N is the first natural frequency of the flexible foil in vacuum, defined as $f_N = k_1^2\sqrt{EI/\rho_s}/2\pi c^2$, where $k_1 = 1.8751$[24].

[c] Symbol "-" indicates that the corresponding parameters are updated during the simulation.

Table I also includes another two key independent parameters, i.e., the Strouhal number (St) and the dimensionless frequency (f^*). St reflects the ratio of the foil's heaving speed to its forward speed, thus characterizes the associated vortex shedding behavior[9]. Typically, St adopted by natural flyers and swimmers varies from 0.2 to 0.4[14], thus it is set as 0.3 in the present study. f^* is a function of the ratio of the foil's effective inertia (defined as m^*k^2/π^2, where m^* is the mass ratio) to its bending stiffness (EI^*), thus dictates the foil's dynamics and the resulting propulsion performance. Our previous study[12] has revealed that the effect of m^* on the foil's propulsion performance is roughly opposite to the effect of EI^*. As such, only the latter, or more exactly, the effect of changing EI^* lower and upper bounds, is examined in this work, while the former is fixed as $m^* = 1$. Furthermore, when f^* is roughly in the range of 0.33 to 0.6, the foil can usually attain an optimal propulsion performance[9,12,25]. Therefore, in this study f^* is selected within this range, i.e., $f^* = 0.52$, when EI^* is moderate, i.e. $EI^* = 3$. Under this condition, $k = \pi/2$ and $h_b^* = \pi St/k = 0.6$, which are applied for all the cases throughout this study.

Equation 7 reveals that the foil's dynamics is determined by the competition among various types of forces/moments, including the inertial force, tension force and bending moment (the three terms on the LHS of Equations 7) as well as the fluid loading (the term on the RHS of Equation 7). Since the foil is assumed inextensible, its deformation is mainly a result of competitions among transverse forces including the inertial force, bending moment and fluid loading. Thus, only these three types of forces/moments are considered, which are evaluated as follows.

As will be revealed in Section III, in the cases of most interest, f^* varies within 1. This means that the foil's deformation is mainly determined by its first bending mode. Under this circumstance, the bending moment usually achieves its maximum at the foil's leading edge, which can be expressed as

$$M_L^* = |EI^* \frac{\partial^2 \boldsymbol{X}^*}{\partial s^{*2}} (t^*, 0)| \tag{12}$$

In this study, M_L^* is defined as positive when the foil is upward-deflected, and negative if the other way around.

For the same reason, the foil's transverse inertial force can be estimated from the y-

component inertial forces at its leading and trailing edges, which are expressed as

$$F^*_{I,L,y} = -\frac{m^* k^2}{\pi^2} a^*_{L,y} \tag{13}$$

$$F^*_{I,T,y} = -\frac{m^* k^2}{\pi^2} a^*_{T,y} \tag{14}$$

where $a^*_{L,y}$ and $a^*_{T,y}$ are the leading- and trailing-edge's y accelerations. Since $a^*_{L,y}$ and $a^*_{T,y}$ are just the second derivatives of the leading- and trailing-edge's y displacements which are either an exact sinusoidal or sinusoidal-like function of time in this study, they are approximately anti-phase with their corresponding y displacements. Thus, the foil's inertial forces are roughly in-phase with its y displacements.

As for the fluid force, it can be evaluated through analyzing the distributed fluid loading along the foil, which will be presented during the discussion. According to Kang *et al.*[9], the fluid force can be decomposed into three major components, namely the viscous force, the vortex force and the acceleration-reaction force. These three types of forces are roughly proportional to three scalings, i.e., $St/2kRe$, $St^2/4k$ and $kSt/2$, respectively, where Re is the Reynolds number which will be fixed at 200 as will be explained in Section II C. Recalling that $St = 0.3$ and $k = \pi/2$, these three scalings are 0.00048, 0.01432 and 0.23562, respectively. This means that the acceleration-reaction is the overwhelmingly dominant factor in determining the fluid loading, whereas the vortices play a negligible role and thus will not be discussed in this study.

To evaluate the foil's propulsion performance and the associated energy consumption under various conditions, two coefficients, i.e., the thrust and energy coefficients, are adopted and defined as

$$C_T = \frac{2F_T}{\rho_f U_\infty^2 c} \tag{15}$$

$$C_E = \frac{2E}{\rho_f U_\infty^2 c^2} \tag{16}$$

where F_T is the thrust and E is the input energy comprising two major components: one is the driven energy applied at the foil's leading edge, which can be attained by integrating the positive power (defined as the positive product of the driving force applied at the leading edge and the leading-edge velocity) over one heaving cycle, and the other is the energy used to realize the bending stiffness rising from the lower bound to the upper bound per heaving cycle.

B. Methodology

To explore the aforementioned FSI problem, the lattice Boltzmann method (LBM)[26] is adopted as an alternative for solving the two-dimensional Navier-Stokes equations. The finite difference method[23,27] is applied to solve Equations 7 and 8 for simulating the structure dynamics. The immersed boundary method (IBM) is integrated with the LBM to resolve the interplay between the fluid flow and the structure dynamics through capturing the structure's motion and evaluating the fluid loading[28]. Details of the current numerical algorithm and its validation can be found in our previous works[12,29,30].

Throughout this study, the computational domain is set as $60c$(L)×$40c$(W) with a uniform flow flowing rightwards with a speed U_∞, as shown in Figure 1(a). The flexible foil is placed $20c$ downstream from the inlet boundary, and the heaving motion imposed at its leading-edge is symmetric about the channel centerline. At the inlet boundary, the non-reflecting inlet boundary condition[31] is used, whereas at the outlet boundary the homogenous Neumann boundary condition is implemented. On the top and bottom walls, the Dirichlet boundary condition is applied with the x velocity U_∞ and y velocity 0.

C. Case summary

According to Section II A, the foil's aerodynamic/hydrodynamic performance mainly depends on the time-dependent bending stiffness which is determined by five parameters including the period T^*_{EI}, the duty cycle D, the phase angle ϕ, and the lower and upper bounds EI^*_{min} and EI^*_{max}. Herein, T^*_{EI} is fixed at 1/2 for simplification, and the focus is mainly placed on exploring the effects of the other four parameters on the foil's propulsion performance. Specifically, seven D values are selected from 0 to 1. ϕ is chosen from 0 to π with an increment $\pi/4$. The ratio of EI^*_{max} to EI^*_{min} is set as 3, a value close to the bending stiffness ratio of eels with unstimulated and stimulated muscles[19]. As such, in this study EI^*_{min} is selected as 1/3, 1 and 3, and EI^*_{max} is set as 1,3 and 9, accordingly. Although the Reynolds number should also play an important role in the foil's aerodynamic/hydrodynamic performance, in this study it is fixed at Re = 200 to focus the discussion, which is slightly larger than the minimum Reynolds numbers adopted by natural swimmers ($O(10^{-2})$)[15] and flyers ($O(10)$)[1]. The selected values for the above parameters are all summarized in Table I.

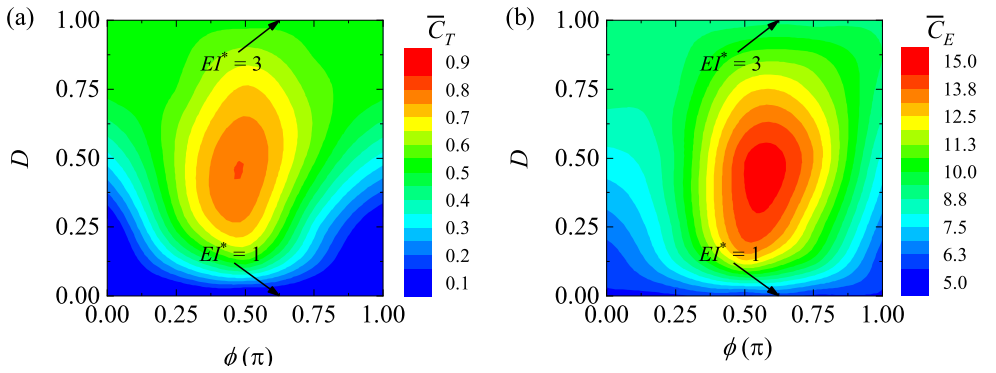

FIG. 2. Contours of the net thrust coefficient ($\bar{C}_T$) (a) and net energy coefficient ($\bar{C}_E$) in the map of the duty cycle (D) versus the phase angle (ϕ) when the bending stiffness (EI^*) is bounded by $EI^*_{min} = 1$ and $EI^*_{max} = 3$.

III. RESULTS AND DISCUSSION

A. Overview of the results

Figure 2 shows contours of the time-averaged thrust coefficient ($\bar{C}_T$) and input energy coefficient ($\bar{C}_E$) in maps spanned by the actuation phase angle (ϕ) and duty cycle (D). In all these cases, the bending stiffness (EI^*) flips between $EI^*_{min} = 1$ and $EI^*_{max} = 3$ in a periodic, square-wave fashion. Note that these two EI^* bounds correspond to non-dimensionless frequencies smaller than 1, indicating that the foil mainly deforms in its first bending mode. As shown in Figure 2(a), the maximum net thrust $\bar{C}_T = 0.8$ is achieved at the map center ($\phi = \pi/2$ and $D = 1/2$), a case where the foil becomes more rigid during strokes and becomes more flexible during stroke reversals. This net thrust is over 2700% and 50% larger than those ($\bar{C}_T = 0.028$ and 0.53) in the constant-bending-stiffness cases with $EI^* = 1$ and 3, respectively, confirming that dynamically adjusting the bending stiffness can significantly improve the foil's propulsion performance. As either the phase angle or the duty cycle deviates from the map center, the net thrust reduces progressively.

If comparing Figure 2(b) with Figure 2(a), it is seen that the contour of the net input energy coefficient is akin to that of the net thrust. This reflects that the more the thrust is enhanced, the more the energy input is required. As a result, the foil's propulsion efficiency defined as their ratio is not significantly improved. For instance, the maximum propulsion efficiency is 6.4% among the cases presented in Figure 2, which is slightly larger than 5.9%

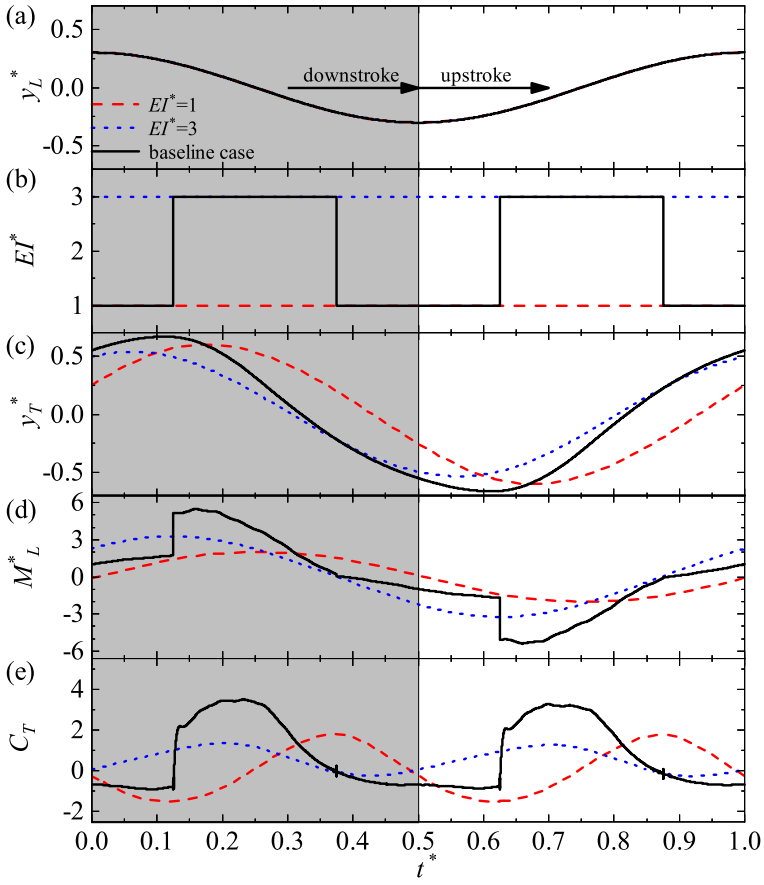

FIG. 3. Time histories of the (a) leading-edge y displacement (y_L^*), (b) bending stiffness (EI^*), (c) trailing-edge y displacement (y_T^*), (d) bending moment at the leading edge (M_L^*), and (e) thrust coefficient (C_T) for the baseline case where EI^*_{min} = 1 and EI^*_{max} = 3 and the cases with the constant bending stiffness, i.e., $EI^* \equiv EI^*_{min} = 1$ and $EI^* \equiv EI^*_{max} = 3$.

obtained in the case with the constant bending stiffness $EI^* = 3$.

B. Effects of dynamically adjusting bending stiffness

To unveil the reasons for the thrust enhancement, in this section the case with $\phi = \pi/2$ and $D = 1/2$ is selected as a baseline case and studied in details. For comparison purpose, the cases with the constant bending stiffness $EI^* = 1$ and 3 are also presented, which are denoted herein as the "flexible" and "stiff" cases, respectively. Since the propulsion performance of the foil with various constant bending stiffness has been systematically studied in our previous work[12], for the sake of brevity we will not repeat the discussions on these two

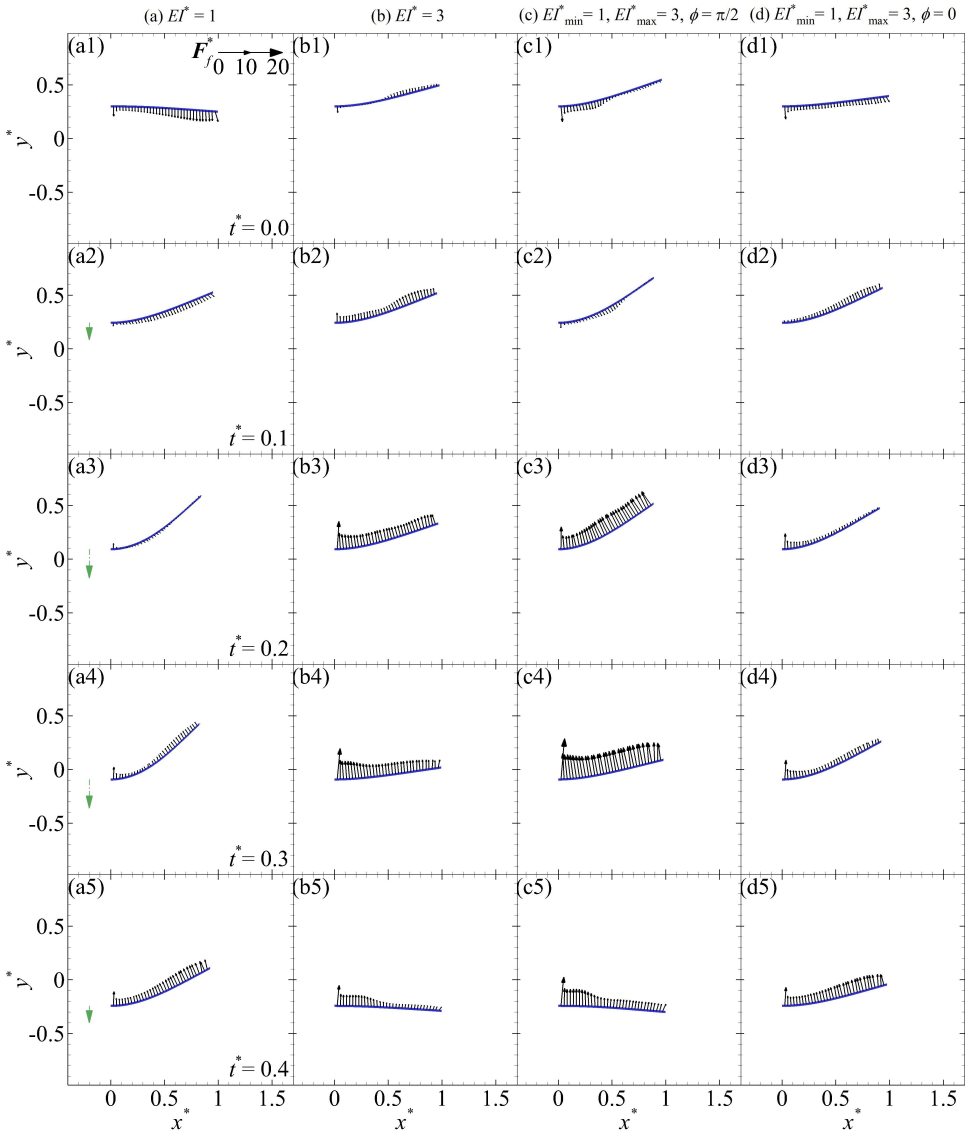

FIG. 4. Distribution of dimensionless fluid stress ($\boldsymbol{F}_f^*$) over the heaving flexible foil during the downstroke in the constant-bending-stiffness cases with EI^* = 1 (a), EI^* = 3 (b), the baseline case where EI^*_{min} = 1, EI^*_{max} = 3 and $\phi = \pi/2$ (c), and the case with EI^*_{min} = 1, EI^*_{max} = 3 and ϕ = 0 (d). The dashed triangle-headed arrow indicates the foil's heaving direction, and its length reflects the heaving speed.

cases. Instead, here we only present their results in Figures 3 and 4 for easy comparison.

Our previous study[12] has revealed that the thrust generation mainly depends on two factors: one is the foil's deflection, and the other is the bending moment that is positively correlated with the foil's shape recovering rate. If the foil has a larger deflection, the fluid loading can contribute more in the upstream direction, favorable for thrust generation (for

example, at around $t^* = 0.4$ in the flexible case, see Figures 3 and 4(a)). On the other hand, larger bending moment can induce larger fluid loading as a reaction force, favorable for thrust enhancement (for example, approximately at $t^* = 0.1$ to 0.3 in the stiff case, see Figures 3 and 4(b)). Note that these two factors are oppositely affected by the bending stiffness, hence they cannot simultaneously exert positive effects in the constant-bending-stiffness cases.

In the baseline case, the bending stiffness remains $EI^* = 1$ at $t^* < 0.125$. Hence, during this period the foil's dynamics is similar to that in the flexible case. Specifically, the foil experiences a larger upward-oriented deflection than that in the stiff case. The bending moment remains small and does not contribute too much to the foil's dynamics. As such, the foil's dynamics is mainly affected by the fluid loading and the inertial force, as indicated by Equations 7, 13 and 14. Under this circumstance, the fluid loading is roughly anti-phase to the inertial force and mainly produces drag, as evidenced in Figures 4(c1) and 4(c2).

At $t^* = 0.125$ when the foil is in its first half of downstroke, the bending stiffness suddenly rises to $EI^* = 3$. With the same deflection, the bending moment is immediately tripled. Owing to that the deflection is larger than that in the stiff case, at this instant the bending moment is enhanced by 57.9%, as shown in Figure 3(d). The sudden rise of bending moment shortly leads to the foil's faster shape recovering process that is accompanied by repelling the fluid downstream and downward in a more intense way. Consequently, the fluid loading quickly reverses its direction and points upwards, becoming even larger than in the stiff case, as revealed in Figures 4(b3) and 4(c3). Furthermore, the foil's larger deflection makes the enhanced fluid loading more upstream-oriented, thus yields much more thrust, as shown in Figure 3(e).

At $t^* = 0.23$, the thrust approaches its maximum $C_T = 3.5$ in the baseline case, 159% larger than that in the stiff case at $t^* = 0.2$. Such a dramatic enhancement completely surpasses the thrust deficiency appearing during the immediately preceding upstroke-to-downstroke reversal, eventually leads to a 50% increase in the net thrust over the stiff case.

At $t^* = 0.375$ when the foil is about to do downstroke-to-upstroke reversal, the bending stiffness drops to $EI^* = 1$. Unlike the instant when the bending stiffness rises, however, this sudden decrease does not invoke obvious change in the foil's dynamics, except that the following bending moment decreasing rate becomes much smaller, as revealed in Figure 3(d). This stems from the fact that at this instant the foil almost recovers its original shape, as evidenced by the nearly identical transverse displacements at the leading and trailing edges

as well as the small M_L^*, as shown in Figure 3.

As time progresses, the foil's shape and all types of forces in the baseline case turns similar to those in the stiff case, as shown in Figures 3, 4(b5) and 4(c5), even though the bending stiffness remains as $EI^* = 1$ in the baseline case. Hence, the foil's dynamics and the thrust generation seem similar in these two cases at around $t^* = 0.4$.

The above discussions suggest that, through dynamically adjusting the foil's bending stiffness at suitable timings as in the baseline case, the two contradicting thrust generation factors can be well utilized to help the foil attain larger deflection and meanwhile experience larger bending moment, yielding a much greater thrust. Furthermore, the larger upward fluid loading during the downstroke indicates that the foil does more work on its surrounding fluid in the baseline case, suggesting the consumption of more energy than in the flexible and stiff cases. Although not shown here for brevity, the fluid loading and resulting energy consumption in the baseline case are also generally greater than those in the other bending-stiffness-varying cases with the same lower and upper bounds. Since both the thrust and the energy consumption are positively correlated to the fluid loading, these two quantities are positively correlated and approach their respective maximums under the same conditions, i.e., in the baseline case, as having been revealed in Section III A.

C. Effect of square-wave phase angle

As revealed in Figure 2(a), the net thrust decreases as the actuation duty cycle and phase angle deviate from the values in the baseline case, i.e., $D = 1/2$ and $\phi = \pi/2$. To unveil the detailed effects of these two parameters, three representative cases, i.e., the case with $D = 1/2$ and $\phi = 0$, the case with $D = 1/8$ and $\phi = \pi/2$ and the case with $D = 7/8$ and $\phi = \pi/2$, are selected and compared for further studies in this and the next sections.

In the case with $D = 1/2$ and $\phi = 0$, the flip of bending stiffness is anti-phase with that in the baseline case, as shown in Figure 5(b). Hence, the small and large bending moments acting on the foil in these two cases are roughly swapped in time. Note that in both cases the foils' locomotion is in phase though, i.e., both the foils undergo small deflections during stroke reversals and large deflections around mid strokes, as revealed in Figures 4(c) and 4(d). As such, in the case with $D = 1/2$ and $\phi = 0$ the foil experiences small deflection when its bending stiffness remains large, i.e., $EI^* = EI^*_{max} = 3$, so that it attains smaller bending

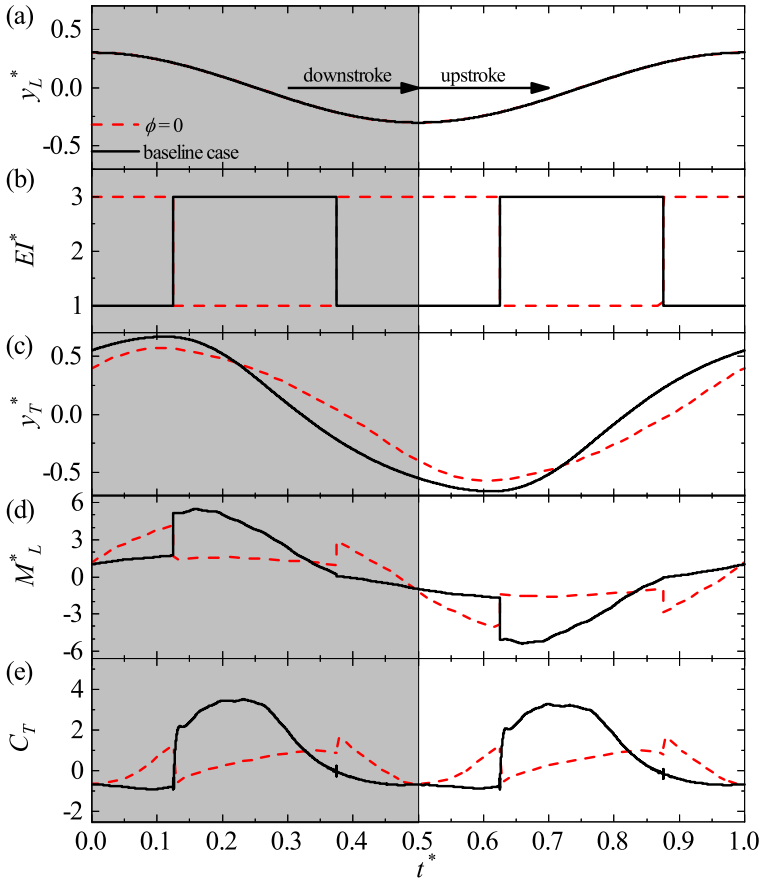

FIG. 5. Time histories of the (a) leading-edge y displacement (y_L^*), (b) bending stiffness (EI^*), (c) trailing-edge y displacement (y_T^*), (d) bending moment at the leading edge (M_L^*), and (e) thrust coefficient (C_T) for the baseline case where $\phi = \pi/2$ and the case with $\phi = 0$, when $EI^*_{min} = 1$ and $EI^*_{max} = 3$.

moment thus smaller thrust than in the baseline case. Furthermore, its bending moment is large during the stroke reversal, imposing more restrictions on the foil's deformation and giving rise to a smaller deflection, and hence further deteriorates the thrust generation. As a result, the net thrust is much smaller in this case.

D. Effect of square-wave duty cycle

As the duty cycle D shrinks to 1/8 or expands to 7/8, the rise or drop of the bending stiffness generally causes changes of the bending moment and the thrust similar to that in the baseline case where $D = 1/2$, as shown in Figure 6. It is seen that, as D increases, the

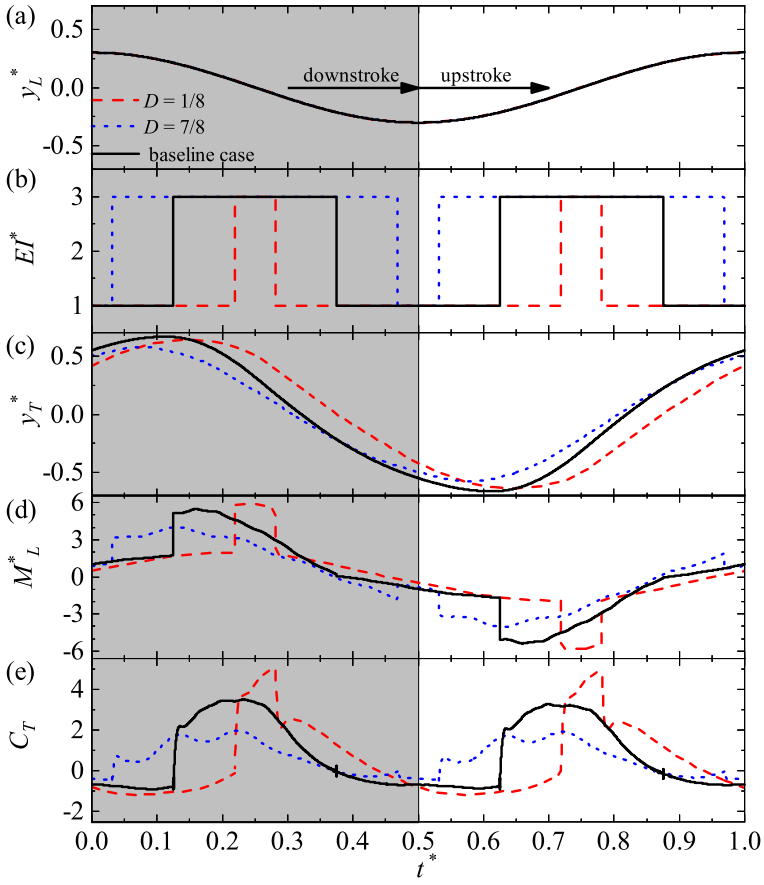

FIG. 6. Time histories of the (a) leading-edge y displacement (y_L^*), (b) bending stiffness (EI^*), (c) trailing-edge y displacement (y_T^*), (d) bending moment at the leading edge (M_L^*), and (e) thrust coefficient (C_T) for the baseline case where D = 1/2 and the cases with D = 1/8 and 7/8, when EI^*_{min} = 1 and EI^*_{max} = 3.

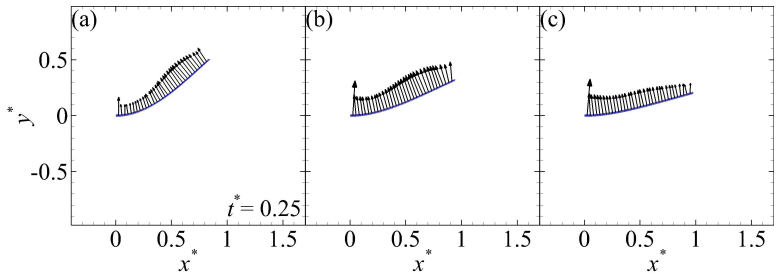

FIG. 7. Distribution of dimensionless fluid stress ($\boldsymbol{F}_f^*$) over the heaving flexible foil at t^* = 0.25 in the case with D = 1/8 (a), the baseline case where D = 1/2 (b), and the case with D = 7/8, when EI^*_{min} = 1 and EI^*_{max} = 3.

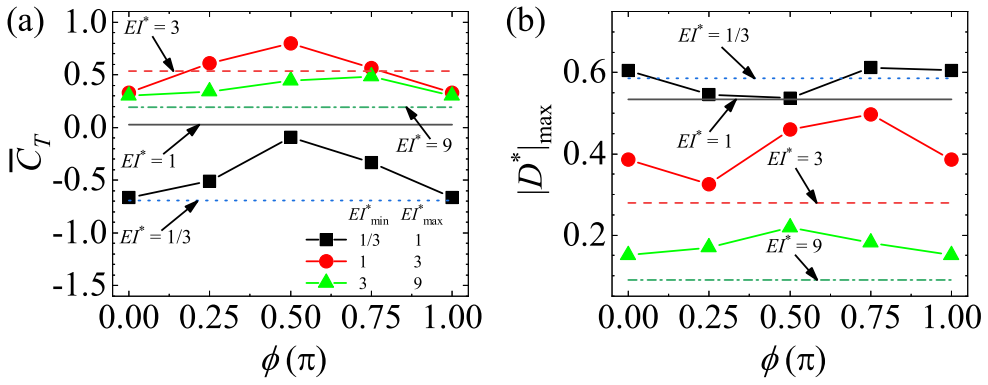

FIG. 8. Net thrust coefficient ($\bar{C}_T$) (a) and maximum deflection ($|D^*|_{max}$) (b) for the cases with time-dependent bending stiffness (represented by the symbol lines) and the corresponding cases with constant bending stiffness (represented by the horizontal lines).

duration for generating positive thrust increases while the peak thrust reduces. This stems from the fact that the large bending stiffness lasts longer as D increases. On one hand, it leads to a longer time for the large bending moment, protracting the duration of the upward- and upstream-oriented fluid loading. On the other hand, the longer large bending moment imposes longer restrictions on the foil during the stroke reversal, resulting in the reduction of the foil's deflection. The reduced deflection then yields less upstream-oriented fluid loading and hence causes a smaller jump in the bending moment and thrust when the bending stiffness rises, leading to a smaller instantaneous thrust, as shown in Figures 6 and 7.

Although it is preferable to increase the instantaneous thrust and in the meantime prolong the large thrust generation when aiming to improve the net thrust, the above observations suggest that only one of these two factors is favored through adjusting the duty cycle. As such, there is a tradeoff between these two factors and the optimal net thrust is attained only when a moderate duty cycle is chosen, which is around $D = 1/2$ in the current study.

E. Effects of bending stiffness

Although dynamically adjusting the bending stiffness (EI^*) bounded by $EI^*_{min} = 1$ and $EI^*_{max} = 3$ can greatly enhance the net thrust, this strategy does not work effectively when these two bounds become smaller or larger. This can be evidenced by the results shown in

Figure 8(a) that the net thrust in the cases with $EI^*_{min} = 1/3$ and $EI^*_{max} = 1$ is less than that in the case with constant $EI^* = 1$, and the net thrust in the cases with $EI^*_{min} = 3$ and $EI^*_{max} = 9$ is less than that in the case with constant $EI^* = 3$.

Unlike in the cases with $EI^*_{min} = 1$ and $EI^*_{max} = 3$ where the large bending moment promotes the thrust generation, in the cases with $EI^*_{min} = 1/3$ and $EI^*_{max} = 1$, the bending stiffness is consistently small so that the bending moment becomes negligible compared to the foil's inertial force and fluid loading. As such, in most of the time the fluid loading is opposite to the inertial force, generating drag instead of thrust.

When $EI^*_{min} = 3$ and $EI^*_{max} = 9$, the foil remains stiff all the time. As a result, its deflection cannot be greatly augmented compared to that in the case with constant $EI^* = 9$, as evidenced by Figure 8(b). Under this circumstance, the fluid loading is more in the transverse direction and thus is not favorable for thrust improvement.

Therefore, in order to effectively enhance the propulsion performance, the lower and upper bounds of the foil's bending stiffness should be moderate so as to allow simultaneous occurrence of adequately enhanced deflection and sufficiently large bending moment, just like in the baseline case.

IV. CONCLUSIONS

This study numerically explores whether dynamically adjusting a heaving foil's bending stiffness (EI^*), in a periodic, square-wave fashion, can enhance the foil's propulsion performance. The major findings are as follows:

1. When EI^* is bounded by $EI^*_{min} = 1$ and $EI^*_{max} = 3$, the net thrust can be enhanced compared to that in the corresponding constant-bending-stiffness cases. The most improvement is achieved in the baseline case, where the EI^* adjusting phase angle $\phi = \pi/2$ and duty cycle $D = 1/2$. The net thrust is enhanced by 2700% and 50% compared to those in the $EI^* \equiv EI^*_{min} = 1$ and $EI^* \equiv EI^*_{max} = 3$ cases, respectively. However, the propulsion efficiency cannot be ameliorated evidently.

2. In the baseline case, the two major thrust-generating factors, i.e., the foil's deflection and bending moment, can be simultaneously improved. As such, the foil attains much larger net thrust.

3. The phase angle determines the timing of the rise of bending stiffness. At $\phi = \pi/2$, EI^* rises when the foil undergoes a large deflection, thus a larger bending moment and thrust can be obtained. As ϕ deviates from $\pi/2$, the foil's deflection reduces, leading to the reduction in the bending moment and net thrust.

4. The duty cycle affects two contradicting factors dictating the net thrust, i.e., the rise of instantaneous thrust and the duration of large thrust generation. As D varies, only one of them is favored. Therefore, a moderate duty cycle around $D = 1/2$ does the best for enhancing the net thrust.

5. When the EI^* bounds become smaller or larger, the foil's bending moment and deflection cannot be simultaneously improved. As such, dynamically adjusting the bending stiffness fails to improve the net thrust.

This investigation confirms that dynamically adjusting the foil's bending stiffness can be beneficial to the thrust generation, which can provide some guidance on the design and operation of newly emerging elastomer actuators in the field of aerodynamics/hydrodynamics. Although insightful, it should be pointed out that the influences of several other important parameters, such as the Strouhal number, the reduced frequency, three-dimensional effect and bending-stiffness waveform, are not explored. All of these will be systematically studied in our near-future work.

ACKNOWLEDGMENTS

We gratefully acknowledge the financial support for this study from the Research Grants Council of Hong Kong under General Research Fund (Project No. 15249316 & 15214418) and the Departmental General Research Fund (Project No. G-UA5A & G-YBLP) from the Department of Mechanical Engineering of The Hong Kong Polytechnic University.

REFERENCES

[1]W. Shyy, Y. S. Lian, J. Tang, D. Viieru, and H. Liu, *Aerodynamics of low Reynolds number flyers*, Vol. 22 (Cambridge University Press, 2007).

[2]C. Ellington, C. Van Den Berg, A. Willmott, and A. Thomas, "Leading-edge vortices in insect flight," Nature **384**, 626 (1996).

[3]M. Dickinson, F. Lehmann, and S. Sane, "Wing rotation and the aerodynamic basis of insect flight," Science **284**, 1954–1960 (1999).

[4]J. Akkala, A. Panah, and J. Buchholz, "Vortex dynamics and performance of flexible and rigid plunging airfoils," J. Fluids Struct. **54**, 103–121 (2015).

[5]K. Lua, S. Dash, T. Lim, and K. Yeo, "On the thrust performance of a flapping two-dimensional elliptic airfoil in a forward flight," J. Fluids Struct. **66**, 91–109 (2016).

[6]K. B. Lua, T. T. Lim, K. S. Yeo, and G. Y. Oo, "Wake-structure formation of a heaving two-dimensional elliptic airfoil," AIAA J. **45**, 1571 (2007).

[7]J. Tang, D. Viieru, and W. Shyy, "Effects of reynolds number and flapping kinematics on hovering aerodynamics," AIAA J. **46**, 967 (2008).

[8]H. Dong, R. Mittal, and F. M. Najjar, "Wake topology and hydrodynamic performance of low-aspect-ratio flapping foils," J. Fluid Mech. **566**, 309–343 (2006).

[9]C. Kang, H. Aono, C. E. S. Cesnik, and W. Shyy, "Effects of flexibility on the aerodynamic performance of flapping wings," J. Fluid Mech. **689**, 32–74 (2011).

[10]X. Zhu, G. He, and X. Zhang, "How flexibility affects the wake symmetry properties of a self-propelled plunging foil," J. Fluid Mech. **751**, 164–183 (2014).

[11]A. M. Lehn, P. J. M. Thornycroft, G. V. Lauder, and M. C. Leftwich, "Effect of input perturbation on the performance and wake dynamics of aquatic propulsion in heaving flexible foils," Phys. Rev. Fluids **2**, 023101 (2017).

[12]C. Wang and H. Tang, "Influence of complex driving motion on propulsion performance of a heaving flexible foil," Bioinspir Biomim **14**, 016011 (2018).

[13]W. Shyy, H. Aono, S. K. Chimakurthi, P. Trizila, C. K. Kang, C. E. S. Cesnik, and H. Liu, "Recent progress in flapping wing aerodynamics and aeroelasticity," Prog. Aerosp. Sci. **46**, 284–327 (2010).

[14]W. Shyy, H. Aono, C. Kang, and H. Liu, *An introduction to flapping wing aerodynamics*, Vol. 37 (Cambridge University Press, 2013).

[15]J. J. Videler, *Fish swimming* (Springer Science & Business Media, 2012).

[16]J. Katz and D. Weihs, "Hydrodynamic propulsion by large amplitude oscillation of an airfoil with chordwise flexibility," J. Fluid Mech. **88**, 485–497 (1978).

[17]S. Heathcote and I. Gursul, "Flexible flapping airfoil propulsion at low reynolds numbers,"

AIAA J. **45**, 1066–1079 (2007).

[18]J. H. Long Jr and K. S. Nipper, "The importance of body stiffness in undulatory propulsion," Am. Zool. **36**, 678–694 (1996).

[19]J. H. Long Jr, "Muscles, elastic energy, and the dynamics of body stiffness in swimming eels," Am. Zool. **38**, 771–792 (1998).

[20]J. J. Videler, *Avian flight* (Oxford University Press, 2006).

[21]B. Gamus, L. Salem, E. Ben-Haim, A. D. Gat, and Y. Or, "Interaction between inertia, viscosity, and elasticity in soft robotic actuator with fluidic network," IEEE Transactions on Robotics **34**, 81–90 (2017).

[22]J. R. Bohnker and K. S. Breuer, "Control of separated flow using actuated compliant membrane wings," AIAA Journal , 1–11 (2019).

[23]W. X. Huang, S. J. Shin, and H. J. Sung, "Simulation of flexible filaments in a uniform flow by the immersed boundary method," J. Comput. Phys. **226**, 2206–2228 (2007).

[24]W. Weaver Jr, S. Timoshenko, and D. Young, *Vibration problems in engineering* (John Wiley & Sons, 1990).

[25]S. Ramananarivo, R. Godoy-Diana, and B. Thiria, "Rather than resonance, flapping wing flyers may play on aerodynamics to improve performance," Proc. Natl. Acad. Sci. U.S.A. **108**, 5964–5969 (2011).

[26]P. Lallemand and L. Luo, "Theory of the lattice boltzmann method: Dispersion, dissipation, isotropy, galilean invariance, and stability," Phys. Rev. E **61**, 6546–6562 (2000).

[27]X. Zhu, G. He, and X. Zhang, "Numerical study on hydrodynamic effect of flexibility in a self-propelled plunging foil," Computers & Fluids **97**, 1–20 (2014).

[28]S. K. Kang, *Immersed boundary methods in the lattice Boltzmann equation for flow simulation*, Ph.D. thesis, Texas A&M University (2010).

[29]C. Wang, H. Tang, S. Yu, and F. Duan, "Control of vortex-induced vibration using a pair of synthetic jets: Influence of active lock-on," Phys. Fluids **29**, 083602 (2017).

[30]C. Wang, H. Tang, S. Yu, and F. Duan, "Lock-on of vortex shedding to a pair of synthetic jets with phase difference," Phys. Rev. Fluids **2**, 104701 (2017).

[31]S. Izquierdo and N. Fueyo, "Characteristic nonreflecting boundary conditions for open boundaries in lattice boltzmann methods," Phys. Rev. E **78**, 046707 (2008).